Effects of atmospheric dynamics and aerosols on the fraction of supercooled water clouds

Jiming Li[1], Qiaoyi Lv[1], Min Zhang[1], Tianhe Wang[1],
Kazuaki Kawamoto[2], Siyu Chen[1] and Beidou Zhang[1]

[1]Key Laboratory for Semi-Arid Climate Change of the Ministry of Education, College of Atmospheric Sciences, Lanzhou University, Lanzhou, China

[2]Graduate School of Fisheries Science and Environmental Studies, Nagasaki University, Nagasaki, Japan

Running Head: Effects of dynamics and aerosols on the cold cloud phase

Corresponding author: Jiming Li, Key Laboratory for Semi-Arid Climate Change of the Ministry of Education, College of Atmospheric Sciences, Lanzhou University, Lanzhou, Gansu 730000, China. (lijiming@lzu.edu.cn)

Abstract

Based on the 8 years' (January/2008-December/2015) cloud phase information from the GCM-Oriented Cloud-Aerosol Lidar and Infrared Pathfinder Satellite Observation (CALIPSO) Cloud Product (GOCCP), aerosol products from CALIPSO, and meteorological parameters from the ERA-Interim products, the present study investigates the effects of atmospheric dynamics on the supercooled liquid cloud fraction (SCF) under different aerosol loadings at global scale to better understand the conditions of supercooled liquid water gradually transforming to ice phase.

Statistical results indicate that aerosols' effect on nucleation cannot fully explain all SCF changes, especially in those regions where aerosols' effect on nucleation is not a first-order influence (e.g., due to low ice nuclei aerosol frequency). By performing the temporal and spatial correlations between SCFs and different meteorological factors, this study presents specificly the relationship between SCF and different meteorological parameters on global scale relatively to the previous studies which mainly focused on special regions. We find that the SCF variation is closely related to the meteorological parameters but their relationship is not stable and varies with the different regions, seasons and isotherm levels. In the tropics, obviously positive correlations between SCFs versus vertical velocity and relative humidity indicate that the higher vertical velocity and relative humidity the larger SCFs. However, the patterns of temporal correlation for LTSS, skin temperature and horizontal wind are relatively more complex than those of vertical velocity and humidity. E.g., their close correlations predominantly locate in middle and high latitudes, and vary with latitude or surface type. Although these statistical correlations haven't been used to establish a certain causal relationship, our results may provide a unique point of view on the phase change of mixed-phase cloud and have potential implications for further improving the parameterization of the cloud phase and determining the climate feedbacks.

1. Introduction

Cloud feedbacks are recognized as the greatest source of uncertainty in the climate change predictions projected by climate models (Boucher et al.,2013). One of the outstanding challenges in better understanding the role of clouds in future climate change involves how to more accurately determine the cloud phase composition between 0 ℃ and -40 ℃. As we know, clouds are composed entirely of liquid or ice particles when temperatures are above the freezing (0 ℃) or below homogeneous freezing (approximately -40 ℃), respectively (Pruppacher and Klett, 1997). Between 0 ℃ and -40 ℃, clouds may be consisted of pure ice, liquid particles or both (that is, mixed-phase). If the temperature of liquid water cloud is lower than 0 ℃, we consider it as supercooled water cloud. The proper partitioning of cloud phase is extremely important to Earth's radiation budget due to differences of cloud liquid and ice in refractive indices, sizes, concentration and shapes (Sun and Shine 1994). For example, by assessing the radiative transfer impacts of mixed-phase clouds, Sassen and Khvorostyanov (2007) showed that the total cloud radiative impact of mixed-phase clouds decreases as supercooled clouds glaciate. In addition, the phase composition also has an important impact on the cloud precipitation efficiency and lifetime (Pinto et al., 1998; Jiang et al. 2000).

Previous studies have verified the existence of supercooled water at temperatures as low as -30 ℃ to -40 ℃ (e.g., Intrieri et al., 2002; Shupe et al., 2006; Morrison et al., 2011). For example, using un-polarized, ground-based Lidar data from Chilbolton in Southern England, Hogan et al. (2003) found that 27% of clouds between -5 ℃ and -10 ℃ in Chilbolton contain a supercooled liquid-water layer; this percentage drops steadily with temperature and reaches approximately zero at temperatures below -35 ℃. Additionally, some observations also showed that the supercooled droplets and ice crystals may survive together in mixed-phase clouds at temperatures as low as -40 ℃ (Borovikov et al., 1963; Sassen 1992). However, the classic Wegener-Bergeron-Findeisen process suggested that coexist of ice crystals and liquid drops in the same volume is colloidally unstable as the cloud ice can quickly grow at

the expense of liquid water due to lower saturation vapor pressure of ice surface (Wegener, 1911; Bergeron, 1935; Findeisen, 1939). Above observation facts possibly indicate that the cloud condensate supplies rate to balance or exceeds the mass diffusional growth rate of ice crystals by vertical motions (Rauber and Tokay, 1991; Forbes and Ahlgrimm, 2014). That is, the persistence of supercooled water layer throughout mixed-phase cloud cycles is directly impacted by the availability of water vapor, concentration and size of ice crystals **(**Rauber and Tokay, 1991; Shupe at al., 2008).

Although temperature dominants the changes of cloud phase composition, its variation is still controlled by other confounding factors, e.g., ice nuclei (IN) (Choi et al., 2010; Tan et al., 2014; Zhang et al., 2015) or dynamical processes (Trembly et al., 1996; Shupe et al., 2007). If large- or meso-scale models are unable to appropriately resolve these microphysical and dynamical processes, they will fail to accurately separate the cloud phase composition, which further affect the major climate feedbacks of global climate models by changing cloud, water vapor, lapse rate and surface albedo (Choi et al., 2014). For example, by conducting a multi-model intercomparison of cloud-water in five state-of-the-art AGCMs, Tsushima at al. (2006) found that the content of cloud ice in the mixed-phase cloud significantly impacts the poleward redistribution of cloud water, thus causes the discrepant cloud albedo feedback among different models. Those models which have less cloud ice in the mixed-phase layer will lead to higher climate sensitivity due to the positive solar cloud feedback. It is therefore of fundamental importance to know the spatiotemporal distributions of different cloud phases, especially supercooled liquid clouds, and their variation with the ice nuclei or environmental conditions changing to improve the simulation of mixed-phase clouds in the current climate models and reduce uncertainties in cloud feedback within models.

Compared with the passive remote sensing (Huang et al., 2005; 2006a), the millimeter-wavelength cloud-profiling radar (CPR) on CloudSat (Stephens et al., 2002) and the cloud-aerosol Lidar with orthogonal polarization (CALIOP) (Winker et al., 2007) on CALIPSO (launched in late April, 2006) can provide more accurate data

regarding the vertical structure of clouds, along with cloud phase information on a global scale (Hu et al., 2010; Li et al., 2010, 2015; Lv et al., 2015). The depolarization ratio and layer-integrated backscatter intensity measurements from CALIOP can help distinguish cloud phases (Hu et al., 2007, 2009). Such as, using combined cloud phase information from CALIOP and temperature measurement from Imaging Infrared Radiometer (IIR), Hu et al. (2010) compiled the global statistics regarding the occurrence, liquid water content and fraction of supercooled liquid clouds. Based on the vertically resolved observations of clouds and aerosols from CALIOP, Choi et al. (2010) and Tan et al. (2014) analyzed the variation of supercooled water cloud fraction and possible dust aerosol impacts at given temperatures. For dynamic processes, although some studies have focused on the impacts of meteorological parameters on supercooled water cloud fraction at regional or global scales (Naud et al., 2006; Cesana et al., 2015), systematic studies of the statistical relationship between cloud phase changes and meteorological parameters at a global scale have received far less attention. For the above reasons, this study combines cloud phase information from the GCM-Oriented Cloud-Aerosol Lidar and Infrared Pathfinder Satellite Observation (CALIPSO) Cloud Product (GOCCP) (Chepfer et al., 2010), meteorological parameters from ERA-interim reanalysis datasets and the aerosol product from CALIPSO to investigate the correlations between supercooled liquid cloud fraction (SCF) and meteorological parameters under different aerosol loadings at a global scale.

This paper is organized as follows: a brief introduction to all datasets used in this study is given in Section 2. Section 3.1 outlines the global distributions and seasonal variations of SCFs and IN aerosol (here, dust, polluted dust and smoke). Further analyses regarding the temporal and spatial correlations between SCFs and meteorological parameters are provided in section 3.2 and 3.3. Important conclusions and discussions are presented in Section 4.

2. Datasets and methods

In the current study, 8 years (January/2008-December/2015) of data from CALIPSO-GOCCP, the ERA-Interim daily product (Dee et al., 2011) and the

CALIPSO level 2, 5 km aerosol layer product are collected to analyze the effects of meteorological parameters on the SCFs under different aerosol loadings at a global scale.

2.1 Cloud phase product

Currently, several methods have been presented to determine the thermodynamic phase at the cloud top based on Lidar-only or combined Radar-Lidar signals. For Radar-Lidar cloud phase products, DARDAR (Delanoe and Hogan, 2010) and CloudSat 2B-CLDCLASS-LIDAR (Zhang et al., 2010) cloud phase products take advantage of the combination of Lidar backscatter and radar reflectivity to distinguish ice clouds, typical mixed-phase clouds, where a liquid top overlies the ice, and liquid clouds. However, Lidar-only method discriminates cloud phase based on the following physical basis. That is, non-spherical particles (e.g., ice crystal) can change the state of polarization of the laser light backscattered, and result in large values of the cross-polarization component ($ATB_{\perp}$) of attenuated backscattered signal (ATB), whereas spherical particles (e.g., liquid droplets) do not.

As a Lidar-only cloud climatology, the main goal of CALIPSO-GOCCP climatology is to facilitate the evaluation of clouds in climate models (e.g., Cesana and Chepfer, 2012; Cesana et al., 2015) with the joint use of the CALIPSO simulator (Chepfer et al., 2008).Thus, GOCCP has been designed to diagnose cloud properties from CALIPSO observations in same way (e.g., similar spatial resolution, same criteria for cloud detection and statistical cloud diagnostics) as in the CALIPSO simulator included in the Cloud Feedback Model Intercomparison Project (CFMIP, http://www.cfmip.net) Observation Simulator Package (COSP) used within version 2 of the CFMIP (CFMIP-2) experiment (Bodas-Salcedo et al., 2011) . This ensures the differences of the observations and the “model+simulator” ensemble outputs are attributed to model biases (Cesana et al., 2015). The CALIPSO-GOCCP cloud algorithm includes following steps. First, the instantaneous profile of the lidar attenuated scattering ratio (SR) at a vertical resolution of 480m is generated from every CALIPSO Level 1 lidar profile (horizontal resolution: 333m). Here, SR is the ratio of the total attenuated backscattered signal (ATB) to the computed molecular

attenuated backscattered signal (ATB_{mol}, only molecules). Then, each atmospheric layer is labeled as cloudy (SR≥5 and ATB-ATB_{mol}>2.5×$10^{-3}km^{-1}sr^{-1}$), clear (0.01≤ SR<1.2), fully attenuated (SR< 0.01) or uncertain pixel (1.2≤SR<5) to construct the three-dimensional cloud fraction. However, it is worth noting that a threshold of 5 for SR in CALIPSO-GOCCP cloud algorithm may miss some subvisible clouds (optical depth<0.03) and result in the underestimation of optical thin cloud layers. Some dense dust or smoke layers also can be misclassified as cloudy pixels (Chepfer et al., 2010). For every cloudy pixel, CALIPSO-GOCCP product is further classified as "ice", "liquid" or "undefined" sample by using the 2-D histograms of ATB, $ATB_{\perp}$ and a phase discrimination line (Cesana and Chepfer , 2013). Those "undefined" samples include three ambiguous parts: (1) cloudy pixels located at lower altitudes than a cloudy pixel with SR>30, (2) cloudy pixels with abnormal value of depolarization (e.g., $ATB_{\perp}$<0 or $ATB_{\perp}$/（ATB-$ATB_{\perp}$）>1), and (3) horizontally oriented ice particles. Cesana and Chepfer (2013) indicated that these "undefined" samples account for about 10.3% of cloudy pixels in 15 months of global statistics. In addition, due to Lidar cannot penetrate optically thick clouds (optical depth>3, such as the supercooled liquid layer in the polar region) to detect ice crystals (Zhang et al., 2010), the CALIPSO-GOCCP cloud phase products possibly lead to a slight underestimation of ice clouds at the lowest levels at Arctic (Cesana et al., 2016).

In the present analysis, the averaged cloud phase information during day- and night-time is derived from the 3D_CloudFraction_Phase_temp monthly average dataset in the CALIPSO-GOCCP v2.9 cloud product. This dataset includes cloud fractions for all clouds ("*cltemp*"), liquid ("*cltemp_liq*"), ice clouds ("*cltemp_ice*") and undefined clouds ("*cltemp_un*") as a function of the temperature in each longitude/latitude grid box (2°×2°). In addition, the temperature used here is obtained from GMAO (Global Modeling and Assimilation Office, Bey et al., 2001), which is part of the CALIPSO level 1 ancillary data. For each CALIOP level 1 profile, the GMAO temperature is interpolated over the 480 m-vertical levels of CALIPSO-GOCCP as the cloudy pixel temperature. That is, the temperature bins are ranged every 3℃ and 38 temperature bins are provided for each parameter. Those

liquid phase clouds whose high bounds of temperature bins are lower than 0 ℃ are considered as supercooled water phase clouds. Similar with the definition of SCF from Choi et al. (2010) and Tan et al.(2014), we calculate the SCF at a given temperature bin (or isotherm) as the ratio of the *cltemp_liq*/(*cltemp_liq*+*cltemp_ice*) in a 2°×2° grid box. Because there is no -10 ℃, -20 ℃ and -30 ℃ isotherms in the CALIPSO-GOCCP product, the present study utilizes the 22th (from -27 ℃ to -30 ℃), 25th (from -18 ℃ to -21 ℃) and 28th (from -9 ℃ to -12 ℃) temperature bins to represent -30 ℃, -20 ℃ and -10 ℃ isotherms, respectively. It is worth noting that this definition may lead to some overestimation of SCFs without considering horizontally oriented ice particles, which is pointed out to account for about 10% of the uncertainty in the study of Choi et al. (2010). However, by analyzing 18 months of CALIPSO data, Noel et al. (2010) demonstrated that the oriented crystals fraction does not seem to be affected by any seasonal effect. Thus, we assume that the oriented crystals would not significantly affect seasonal cycles of SCF and our results despite of some uncertainties in present study.

2.2 Meteorological reanalysis dataset

The ERA-Interim reanalysis daily 6-hour products are also used here to provide the related information of meteorological parameters at the surface and several pressure levels, including the skin temperature, surface pressure and 2-m air temperature at surface level, vertical velocity at 500-hPa level, the U component of wind at 100-hPa level, temperature at 700-hPa level, and relative humidity at three levels (400-, 500- and 600-hPa). Note that all these variables are matched with the CALIPSO aerosol product in space and time to perform correlation analyses with SCFs in section 3.2 and 3.3. Here, the 700-hPa temperature, surface- and 2-m air temperature are used to calculate the lower-tropospheric static stability (LTSS), which is defined as the difference in potential temperature between 700-hPa and the surface (Klein and Hartmann, 1993), as described below:

$$\Delta\theta = T_{700}\left(\frac{1000}{p_{700}}\right)^{R/C_p} - T_{sfc}\left(\frac{1000}{p_{sfc}}\right)^{R/C_p} \quad (1)$$

where p presents pressure, T is temperature, R and C_p denote the gas constant of air,

and the specific heat capacity at a constant pressure respectively. Note that, a high LTSS value represents a stable atmosphere and the positive vertical velocity implies updraft in this study, and vice versa.

2.3 Aerosol types and relative frequency

Aerosol data is obtained from the CALIPSO level 2, 5 km aerosol layer product. Using scene classification algorithms (SCAs), CALIPSO first classifies the atmospheric feature layer as either a cloud or aerosol by using the mean attenuated backscatter coefficients at 532/1064 nm, along with the color ratio (Liu et al., 2009). A confidence level for each feature layer is also supplied by the level 2 products. Using the surface type, Lidar depolarization ratio, integrated attenuated backscattering coefficient and layer elevation, aerosols are further distinguished as desert dust, smoke, polluted dust, clean continental aerosol, polluted continental aerosol, and marine aerosol (Omar et al., 2009). Mielonen et al. (2009) used a series of Sun Photometers from the Aerosol Robotic Network (AERONET) to compare CALIOP and AERONET aerosol types and found that 70% of the aerosol types from these two datasets are similar, especially for the dust and polluted dust types. Mineral dust from arid regions has been widely recognized as an important source of ice nuclei in mixed-phase clouds because of its nucleation efficiency and abundance in the atmosphere (Richardson et al., 2007; DeMott et al., 2010; Atkinson et al., 2013). In addition to dust, some studies have also verified the potential ice nucleation ability of polluted dust and smoke at cold temperatures (Niedermeier et al., 2011; Cziczo et al., 2013; Tan et al., 2014; Zhang et al., 2015). Therefore, we calculate the total relative occurrence frequency (RAF) of these IN aerosol types by combining the dust, polluted dust and smoke information from CALIPSO here. Given the difficulty of quantifying the concentration of IN aerosols, the relative occurrence frequency can be used as a proxy of the concentration of aerosols (Choi et al., 2010). In addition, those aerosol layers with low confidence values (feature type QA flag is "low" in aerosol product) are removed from the dataset (approximately 6.5% of all aerosol layers). Meanwhile, GMAO temperature of aerosol layer-top is also used here to select consistent temperature bins with the CALIPSO-GOCCP cloud product. For every IN aerosol

sample, we arrange a temperature bin based on its layer-top temperature. Then, we define the frequency of IN aerosols at a given temperature bin as the ratio of the number of IN aerosol samples to the total number of observation profiles for the same temperature bin and grid (Choi et al. 2010). Finally, the relative occurrence frequencies of IN aerosols are calculated by normalizing aerosol frequencies. That is, aerosol frequencies are divided by the highest aerosol frequency at a given isotherm (that is, temperature bin). The RAF is thus indicative of the temporal and spatial variability of IN aerosols compared to the maximum occurrence frequency (Choi et al., 2010).

Furthermore, considering the sparse sample data for the narrow CALIOP orbit, we reduce the horizontal resolution from 2 °to 6 °for ensuring enough samples in each grid box when analyzing the relationship between SCFs and meteorological parameters under different aerosol loadings (section 3.2). To avoid artifacts due to noise from scattering of sunlight, it is better to conduct the CALIOP retrieval during nighttime. However, in view of the lack of CALIPSO observations at high latitudes of the northern Hemisphere during boreal summer nights, this study utilizes the mean values of SCFs, meteorological parameters and RAFs during daytime and nighttime to perform the temporal and spatial correlations analysis.

3 Results

3.1 Global and seasonal distributions of 8-year average SCFs and RAFs

Based on the statistical results of the 8-year CALIPSO-GOCCP cloud phase product and CALIPSO level 2-5 km aerosol layer product, the global distributions and seasonal variations of SCFs and the RAFs of aerosol at three isotherms, i.e., −10ºC, −20ºC, and −30ºC, at a 2º latitude by 2º longitude resolution are provided in Fig. 1-3, respectively. At the -10 ℃ isotherm (Fig. 1), supercooled water cloud fractions are large at middle and high latitudes of two hemispheres. Especially, the SCFs are exceed 70% over the high latitudes (poleward of 60 °) except for Greenland during all seasons. The SCFs between 30 °N and 30 °S range from 15% to 50% approximately; the lowest SCFs (<30%) are predominantly located in typical subsidence regions (e.g., stratocumulus regions), where weak subsidence favors low cloud formation and

suppresses mixed-phase cloud generation (Wood et al., 2012; Yuan and Oreopoulos, 2013). Moreover, low SCFs also occur in the northwest part of China during boreal spring and winter. For relative aerosol frequency at the -10 ℃ isotherm, its global distributions are expected and large RAFs are predominantly located in the dust source regions, i.e., Saharan and Taklimakan Deserts, where dust relative frequencies are greater than 20% during boreal summer and spring, respectively. The "aerosol belt" near America (between 30 ℃N and 60 ℃N) during boreal spring is mostly from the long-range transport of dust from the Taklimakan Desert, which travels across the Pacific Ocean to America via westerlies (Huang et al., 2008). In addition, Saharan dust can also be transported by trade winds across the Atlantic to America and the Caribbean. At the −20ºC and -30 ℃ isotherms, the spatial distributions of SCFs are similar to those results at -10 ºC, and SCFs are lower at −20 ℃ and -30 ℃ than at −10ºC. However, the seasonal variation of SCFs at −20ºC and -30 ℃ are more obvious compared with those results at −10ºC, especially at high latitudes of the northern hemisphere. For RAFs, however, note that comparison between different isotherms is not meaningful because the RAFs are normalized relative to each fixed isotherm. Thus, larger RAF at -20 ℃ or -30 ℃ than at -10 ℃ does not mean that the true aerosol frequency at -20 ℃ or -30 ℃ is really higher than values at -10 ℃. Compared with the RAFs at the -10ºC isotherms, the “aerosol belt” between 30° and 60° for two hemispheres at the -20 ℃ or -30 ℃ isotherms is more apparent. Previous studies have verified that the regional differences in the SCFs at -20 ℃ or other isotherms are highly correlated with the dust frequency above the freezing level (Choi et al., 2010; Tan et al., 2014). However, based on Figs. 1-3, we find that this is not always the case for all regions. For example, the SCFs in the tropics maintain persistently low values at three isotherms throughout the whole year, even though the aerosol loading is very low in this region. Moreover, by analyzing the zonal means of SCF and RAF (Fig. 4), we find that the SCF still has a low value at the mid-latitudes of the northern hemisphere during the summer season, even though the IN aerosol loading is significantly low at -20 ℃ over these regions. The obvious seasonal variations of SCFs over these regions seem not to be explicitly related to the seasonal variation of aerosol

frequency. These results indicate that the aerosols' effect on nucleation cannot fully explain all changes of the supercooled liquid cloud fraction in our study, especially its regional and seasonal variations. In other words, there is no evidence to suggest that the aerosol effect is always dominant at each isotherm or region. Then, can these variations of SCF attribute to the meteorological effect? If yes, what is the role of meteorological parameters on the cloud phase change, especially at those regions in which the aerosol effect on nucleation isn't first-order due to low IN aerosol frequency? In the following section, temporal and spatial correlation analysises between SCFs and meteorological parameters are conducted to help discuss these questions.

3.2 Temporal Correlations between SCFs and meteorological parameters

Synoptical-scale dynamics is the first order variable driving the formation of clouds and their properties (Noel et al., 2010). Aside from temperature, some past studies and observations already verified the updraft motions can supply a plentiful of water vapor for the persistence of cloud liquid, thus play an important role on the cloud phase partitioning in the mixed-phase clouds (Rauber and Tokay, 1991; Tremblay et al., 1996; Shupe at al., 2006). A sufficient updraft can be sourced by cloud top entrainment of dry air, radiative cooling, wing shear, larger-scale instabilities, and surface turbulent heat fluxes (Pinto 1998; Moeng 2000). In addition, Naud et al. (2006) also indicated that glaciation of supercooled water drops may be a function of the vertical motions, precipitation, development stage of cloud and concentration of ice nuclei. In this section, we investigate the potential correlations between meteorological parameters and SCF over the 8-year period (96 months). Although these statistical correlations don't imply all the causation, we expect that these results may provide a unique point of view on the phase change of mixed-phase cloud.

In view of the issue of a sparse dataset caused by the narrow orbit of CALIOP, we perform the correlation analysis at 6 °latitude by 6 °longitude grid boxes. Firstly, we calculate the monthly averages of SCF, meteorological parameters and RAFs at different isotherms (or pressure levels) in each 6 °latitude by 6 °longitude grid box by

using the following equation: $\overline{M} = (\sum_{i=1}^{9} w_i \times M_i) \Big/ \sum_{i=1}^{9} w_i$. Where M_i is the averaged SCF or meteorological parameters of the i_{th} 2°×2° grid box in this 6°×6° geographic region, and $w_i = \cos(\theta_i \times \pi / 180.0)$, here θ_i is the mean latitude of the i_{th} 2°×2° grid. Then, temporal correlations between monthly averaged SCF and meteorological parameters are provided in each 6° latitude by 6° longitude grid box. It is worth noting that only those regions whose temporal correlations are at the 90% confidence level are displayed in the following global maps, and are used further to discuss the spatial correlation in section 3.3.

Fig. 5 shows the global distributions of temporal correlations between SCFs at three isotherms (-10 ℃, -20 ℃ and -30 ℃) and skin temperature, vertical velocity at 500-hPa. For skin temperature (left panel), temporal correlation coefficients have obvious regional differences. For example, at the -10 ℃ isotherm, negative temporal correlations mainly locate in Europe and ocean regions between 30° and 60° of two hemispheres, whereas the positive correlations can be found in the tropics, Mainland China, and Greenland. The positive correlation implies that seasonal cycles of skin temperature are consistent with those of SCF, whereas negative correlation indicates that their seasonal cycles are opposite. In the tropics, high skin temperature tends to trigger tropical deep convection easily. The vigorous updrafts in convective clouds do not leave enough time for supercooled droplets to transform into ice crystals, thus suppressing ice formation or pushing supercooled liquid water to a colder cloud top height (Bower et al., 1996). Indeed, the obvious positive temporal correlations in the tropics between SCFs and the vertical velocity at 500-hPa provide support for this inference. In addition, vigorous ascent brings a plentiful of water vapor from the tropical sea surface to high level can also maintain the liquid layer of convective clouds if IN concentrations are small (Rauber and Tokay, 1991). However, Figs.1-3 all show that the tropics have the lowest SCFs in the world at any isotherm. This result is consistent with the previous study of Hu et al. (2010). We consider the possible reasons as: (1) The CALIOP can't penetrate the optically thick clouds (optical depth>3)

to detect the lower clouds, especially over the tropics where cloud overlap is very frequent (Li et al., 2015). (2) This study focuses on the cloud top phase of mixed-phase cloud as well as pure ice or liquid clouds. It implies that frequent tropical ice cloud may result in low SCF. (3) Those regions with lowest SCF usually correspond to the typical descending motion. In these moderate or strong subsidence regions, the cloud occurrence is infrequent at the atmospheric layer between -40 ℃ to 0 ℃. However, a little high cloud (or ice phase cloud) still can exist at this layer. The major source of these high clouds is topography-driven gravity wave activity, advection from neighboring tropical convection centers such as the Amazon Basin, the Congo Basin, or the ascent associated with mid-latitude fronts (Yuan and Oreopoulos, 2013). Thus, positive correlation between SCF and velocity also exists at subsidence regions with low SCF. At middle latitudes, we find a negative correlation between SCF and surface temperature except for Mainland China. It means that low SCF corresponds to warm surface temperature. By analyzing the frontal clouds over the mid-latitudes of northern hemisphere, Naud et al. (2006) pointed out that the changes in glaciation temperature of supercooled liquid cloud appear to be related to the sea surface temperature (SST) pattern, storm vertical velocity and strength. Glaciation is likely to occurs preferentially in the storm region where the warmer SST occurs. In these warm regions, strong precipitation rates exhaust the supercooled liquid drops. Their finding possible partially explains the negative correlations between SCF and skin temperature at the mid-latitudes in our study. However, we find that opposite correlations between SCF at -10 ℃ isotherm and surface temperature exist at middle and high latitudes, but seasonal cycles of surface temperature at these two latitudinal zones are similar. It shows that SCFs at middle and high latitudes have inverse seasonal variations, which is unable fully interpreted by the surface temperature. By analyzing the time series of other parameters, the opposite seasonal variations of SCF at these two latitudinal zones seem are correlated with atmospheric stability (e.g., LTSS). At high latitudes of southern hemisphere, the vertical motion is relatively weak and the atmosphere is stable (high LTSS), thereby cannot supplying sufficient moist to the liquid layer of mixed phase cloud. With decreasing temperature

(e.g., at the -20 ℃ isotherm), the negative temporal correlation coefficients between SCFs and skin temperature are more obvious at middle and high latitudes. But, the correlations disappear at -30 ℃ isotherm, which are also seen in Fig.6 and 7. It is mainly due to that the seasonal cycles of SCF at this isotherm are unapparent or even opposite to other isotherms (e.g., eastern part of Russia or Greenland).

Cesana et al. (2015) found that rising air supports the ice crystals formation over liquid droplets for decreasing temperatures. The same trend is observed at different latitudes (tropics, midlatitudes, and poles). However, West et al. (2014) concluded that the subgrid vertical velocity enhancing leads to an increase of the liquid water path. In this study, our results indicate that obvious positive correlations (greater than the 90% confidence level) between SCFs and 500-hPa vertical velocity only locate in tropics (right panel of Fig.5). There are some negative correlations at middle and high latitudes, but the confidence level is very low. Some studies already verified the importance of vertical motions for supporting the growth of liquid water in Arctic mixed-phase clouds (Shupe et al., 2006; 2007). However, the correlation in our study is unapparent. It might be because large grid sizes in this study miss many cloud-scale vertical motions.

Following Fig. 5, Fig. 6 shows the temporal correlations between SCFs at three isotherms and LTSS, relative humidity at three pressure levels (400-hPa, 500-hPa and 600-hPa). It is clear that SCF at tropics apparently positive correlate with humidity. By analyzing the time series of perturbation for SCF and humidity (figure not shown), we find that their correlation is still obvious at tropics. Based on the low relative occurrence frequency and weak seasonal cycle of IN aerosols at different isotherms of tropics, our results indicate that seasonal variations of SCFs at a given isotherm can be attributed to the effect of meteorological parameters, especially the relative humidity. Besides the humidity, there is also obvious correlation between SCF and LTSS (right panel of Fig.6). We can see that the negative correlations between SCFs and LTSS mainly locate at the ocean region. It means that SCF is low in a stable low level atmosphere. For the horizontal wind speed at 100-hPa, Noel et al. (2010) found that the frequency of oriented crystal drops severely in areas dominated by stronger

horizontal wind speed at 100-hPa. This effect is especially noticeable at latitudes below 40°. But, they have not explained why the correlation between horizontal wind speed and horizontally-oriented ice particle is negative. We speculate that strong horizontal wind possibly results in strong vertical wind shear, thus cause shear-gravitational wave motions to induce local updraft circulations (Rauber and Tokay, 1991). As a result, updraft possibly perturbs the orientation of ice crystal. In addition, Westbrook et al. (2010) pointed out that supercooled liquid water layers is very important in the formation of planar ice particles which are susceptible to orientation at midlatitudes. Based on these studies, we assume that the temporal correlation between SCF and zonal wind speed also exists. Indeed, stronger winds are correlated with an increase in SCFs at different isotherms for middle latitudes, whereas negative correlations also exist in central Africa, the Tibetan Plateau or poleward regions of 60°S (see Fig.7). All this being said, this section presents specificly the relationship between SCF and different meteorological parameters on global scale relatively to the previous studies which mainly focused on special regions, although we have not established a certain causal relationship in present study. Noticeably, our statistical results demonstrate that the SCF variation is closely related to the meteorological parameters but their relationship is not stable and varies with the different regions, seasons and isotherm levels, which is should be treated carefully in the prediction of future climate change.

Furthermore, we select three regions represent different aerosol loadings and investigate their temporal variations of SCFs, meteorological parameters and RAFs of IN aerosol in several selected regions in Fig. 8-10, respectively. Note that each line in every subplot is dealt with 5-month running mean, and the coefficients in title, however, is calculated based on the original series, which is greater than 90% confidence level. We also provide the confidence value (i.e., p value) when the confidence level of the temporal correlation between variables is less than 90%. Fig. 8 shows the time series of various variables at the -30℃ isotherm over the central China (102°E-108°E, 30°N-36°N), which is nearby the Taklimakan Desert. High frequencies of dust and polluted dust in this region peak during the months when SCFs are at

minimum with the correlation coefficient of -0.44. Negative correlations also exist between SCF and LTSS (or horizontal wind at 100-hPa); their values are -0.18 and -0.44, respectively. In addition, the skin temperature over this region also display a coherent seasonal variation with the SCFs (corrcoef=0.44). At the -10 ℃ isotherm over a region near the Bahamas (66 ℃W-60 ℃W, 18 ℃N-12 ℃N), the RAFs of aerosol are persistently low (<0.02) for 96 months (see Fig.9). The correlation coefficient between SCF and RAF is only 0.01, and its confidence level is very low (P=0.89). The obvious seasonal variations of SCF over this region are high consistent with the meteorological parameters. E.g., their correlation coefficients are 0.53, 0.47 and 0.65 for skin temperature, vertical velocity and relative humidity, respectively. The third region is located over the southern ocean (84 ℃E-90 ℃E, 54 ℃S-60 ℃S), where the maximum RAF of aerosol at the -20 ℃ isotherm can reach 0.06 (see Fig.10). Skin temperature and LTSS have negative correlations with SCF (-0.35 and -0.49, respectively), whereas a positive temporal correlation exists between SCF and U wind (approximately 0.37). These statistical results further indicate that the same meteorological parameter has a distinct correlation with SCFs in different regions.

3.3 Spatial Correlations between SCFs and meteorological parameters

In this section, we further investigate the spatial correlations of SCF and different meteorological parameters at tropics (30 ℃N-30 ℃S) and middle-high latitudes (90 ℃N-30 ℃N; 30 ℃S-90 ℃S) under different aerosol loadings. As demonstrated in section 3.2, the relationship of the meteorological parameters and SCF is unstable and vary in different regions. For example, the significant correlation (at the 90% confidence level) appears at tropics (30 ℃N-30 ℃S) for the SCF and velocity (or humidity), but occur at middle or high latitudes for zonal wind. Thus, we mainly discuss the vertical velocity at 500-hPa, relative humidity and skin temperature at tropics, and LTSS, zonal wind at 100-hPa and skin temperature at middle and high latitudes. Here, each meteorological factor of grids is grouped into six bins based on its values within a specified aerosol loading level. In the present study, the aerosol loadings are divided into three levels based on relative aerosol frequencies. However, in view of the apparent difference of aerosol loading level between the tropics and middle-high

latitudes, different thresholds are used. For the tropics, aerosol levels include: high level (RAF>0.025), middle level (0<RAF<0.025) and low level (RAF=0). For middle-high latitudes of southern hemisphere, the three aerosol levels are high level (RAF>0.025), middle level (0<RAF<0.025) and low level (RAF=0). Instead, three aerosol levels are high level (RAF>0.12), middle level (0<RAF<0.12) and low level (RAF=0) at middle-high latitudes of northern hemisphere, respectively. Such grouping ensures a sufficient number of samples available in each bin (at least hundreds of samples in each bin) to satisfy statistical significance. Moreover, note that only regions with temporal correlations of SCFs and meteorological parameters greater than the 90% confidence level are used to calculate the spatial correlations between SCFs and meteorological parameters.

Fig. 11 shows clearly the different spatial correlations between SCF at the -20 ℃ isotherm and the meteorological parameters for different latitudes. The error bars correspond to the ±5 standard error. Here, the standard error (SE) is computed as: $SE = SD/\sqrt{N}$, where SD is the standard deviation of the data falling in a meteorological parameter bin (e.g., vertical velocity <-10 hPa/day) and aerosol loading level; N is the sample number in each bin. At a fixed isotherm (such as, -20 ℃) of tropics, we may find that SCFs and 500-hPa vertical velocity (or relative humidity at 500-hPa level) have a significantly positive correlation spatially at the 90% confidence level under different aerosol loading. However, the low correlations and confidence level (see Table 1) in Fig. 11c verify that the obvious spatial correlation vanishes for skin temperature. Moreover, we also note that there is no evident correlation between SCFs and aerosol loading levels under the same meteorological conditions in the tropics. By performing a similar analysis at different isotherms and aerosol thresholds, we confirm this conclusion. The spatial correlation coefficients between SCFs and meteorological parameters at three isotherms are summarized in Table 1. The statistical results thus indicate that the changes of tropical SCFs at a given isotherm are positive correlated with vertical velocity and relative humidity. Aerosol's effect can't fully interpret the seasonal cycles of SCF. However, the

significance level of their spatial correlations decreases with decreasing temperature, especially at -30 ℃ isotherms (see Table 1). For the middle-high latitude of northern hemisphere, however, the obvious spatial correlations mainly exist between SCFs and zonal wind at 100-hPa and skin temperature. In summary, strong horizontal wind and low skin temperature (or stable lower-layer atmosphere) corresponds to high SCF. But, we find that SCFs under high aerosol loading aren't lowest as we expected, especially at the southern hemisphere. This result isn't consistent with the previous study of Tan et al. (2014), which demonstrated that SCFs and RAFs of dust, polluted dust and smoke are not only temporally negatively correlated but also spatially negatively correlated. The possible reason is that their results only include those grids with confident correlation between SCF and RAF. Based on Fig.2 and 3, we find that the SCF at southern ocean is very high, whereas the aerosol frequency isn't lowest over this region. This further indicates that aerosol isn't the unique factor to affect the seasonal cycles of SCF. For LTSS, opposite spatial correlations exist at different hemispheres (see Fig.11d and 11g). Based on Fig. 6 and 11, we speculate that the negative part of the correlation possibly corresponds to ocean regions, whereas the positive part of the correlation mainly corresponds to land regions (such as Siberia and America). Here, we emphasize that the statistical relationships between SCFs and meteorological parameters are based on the long- time (96 months) datasets to ensure the correlations at the 90% confidence are robust. From above analysis and discussion, we certain that, at least, meteorological parameters impact the variation of SCFs at a given isotherm for those clear regions, and their impacts depend on regions.

4. Conclusions and Discussion

Changes in cloud phase can significantly affect the Earth’s radiation budget and global hydrological cycle. Based on the 8 years (2007-2015) of cloud phase information dataset from CALIPSO-GOCCP, aerosol products from CALIPSO, and meteorological parameters from the ERA-Interim, this study investigates the effects of atmospheric dynamics on the supercooled liquid cloud fraction under different aerosol loadings at a global scale and achieve some new insights in this paper.

Previous studies mainly focused on warm water cloud systems (Li et al., 2011,

2013; Kawamoto and Suzuki, 2012, 2013) or dust properties retrieval and simulations (Huang et al., 2010; Bi et al., 2011; Liu et al., 2011) or have demonstrated the importance of dust with respect to cloud properties (Huang et al., 2006b, 2006c, 2014; Su et al., 2008; Wang et al., 2010; 2015; 2016). Some studies have investigated the impact of different aerosol types on cold phase clouds over East Asia (Zhang et al., 2015) or at a global scale (Choi et al., 2010; Tan et al., 2014). However, systematic studies of the statistical relationship between cloud phase changes and meteorological parameters have received far less attention, especially at a global scale. To clarify the roles of different meteorological factors in determining cloud phase changes and further provide observational evidence for the design and evaluation of a more physically based cloud phase partitioning scheme, we perform specificly temporal and spatial correlations between SCFs and different meteorological factors on global scale in this work.

Statistical results indicate that aerosols' effect on nucleation cannot fully explain all SCF changes, especially in those regions where aerosols' effect on nucleation is not a first-order influence (e.g., due to low IN aerosol frequency). The meteorological parameters also play important roles on the SCF variation. However, the statistical relationship between meteorological parameters and SCF is not stable and varies with the different regions In the tropics, obvious positive correlations between SCFs and vertical velocity (or relative humidity) indicate that seasonal cycles of vertical velocity (or relative humidity) are consistent with those of SCFs. However, the impacts of LTSS, skin temperature and horizontal wind on SCFs are relatively complex than those of vertical velocity and humidity. Their temporal correlations with SCFs depend on latitude or surface type. For example, at the -10 ℃ isotherm, negative temporal correlations for skin temperature mainly locate in Europe and ocean regions between 30 ° and 60 ° for two hemispheres, whereas positive correlations can be found in the tropics, Mainland China and Greenland. With decreasing temperature (e.g., at the -20 ℃ isotherm), temporal correlation coefficients between SCFs and skin temperature are almost negative in middle and high latitudes. However, it is clear that their temporal correlations also gradually weaken (even vanish) with decreasing

temperature. By analyzing the spatial correlations under different aerosol loadings, we find that positive correlations also exist between SCF and the vertical velocity (or humidity) in the tropics, whereas no evident correlation exists between SCFs and aerosol loading levels under the same meteorological conditions in the tropics. At middle and high latitudes, the obvious positive (or negative) spatial correlations mainly occur between SCFs and u wind at 100hPa (or skin temperature). Recently, there is evidence has shown that a cloud phase feedback occurs, causing more shortwave to be reflected back out to space relative to the state prior to global warming (McCoy et al., 2014; 2015). Our results, which are based on long- times' (96 months) global observations verify the effects of dynamic factors on cloud phase changes and illustrate that these effects are regional, thus have potential implications for further reducing the biases of climate feedbacks and climate sensitivity among climate models.

Acknowledgments.

This research was jointly supported by the key Program of the National Natural Science Foundation of China (41430425), Foundation for Innovative Research Groups of the National Science Foundation of China (Grant No. 41521004), National Science Foundation of China (Grant No. 41575015 and 41305027) and the China 111 project (No. B13045). We would like to thank the CALIPSO-GOCCP, CALIPSO and ERA-Interim science teams for providing excellent and accessible data products that made this study possible.

References

Atkinson, J. D., Murray, B. J., Woodhouse, M. T., et al.: The importance of feldspar for ice nucleation by mineral dust in mixed-phase clouds, Nature, 498, 355-358, 2013.

Boucher, O., et al.: Clouds and aerosols, in Climate Change 2013: The Physical Science Basis. Contribution of Working Group I to the Fifth Assessment Report of the Intergovernmental Panel on Climate Change, edited by T. F. Stocker et al.,

pp. 571–657, Cambridge Univ. Press,Cambridge, U. K., and New York, doi:10.1017/CBO9781107415324, 2013.

Bergeron, T.,: On the physics of cloud and precipitation, Proc. Fifth Assembly UGGI Lisbon, Vol. 2, Lisbon, Portugal, UGGI, 156–173, 1935.

Bey, I., Jacob, D. J., Yantosca, R. M., Logan, J. A., Field, B. D., Fiore, A. M., Li, Q., Liu, H. Y., Mickley, L. J., and Schultz, M. G.: Global modeling of tropospheric chemistry with assimilated meteorology: Model description and evaluation, J. Geophys. Res., 106(D19), 23, 073–23,095, doi:10.1029/2001JD000807, 2001.

Bi J., Huang, J., Fu, Q., Wang, X., Shi, J., Zhang, W., Huang, Z., and Zhang, B.: Toward characterization of the aerosol optical properties over Loess Plateau of Northwestern China, J. Quant. Spectrosc. Radiat. Transf., 112, D00K17, doi:10.1029/2009JD013372, 2011.

Borovikov, A. M., Gaivoronskii, I. I., Zak, E. G., Kostarev, V. V., Mazin, I. P., Minervin, V. E., Khrgian. A. Kh. and Shmeter, S. M. 'Clouds physics'. Israel Program for Scientific Translation. Available from US Dept. of Commerce, Washington, DC, USA, 1963.

Bower, K. N., Moss, S. J., Johnson, D.W., Choularton, T.W., Latham, J., Brown, P. R. A., Blyth, A.M., and Cardwell, J.: A parameterization of the ice water content observed in frontal and convective clouds, Quart. J. Roy. Meteor. Soc., 122, 1815–1844, 1996.

Bodas-Salcedo, A, et al.: COSP: Satellite simulation software for model assessment, Bull. Am. Meteorol. Soc., 92, 1023–1043, doi:10.1175/ 2011BAMS2856, 2011.

Cesana, G., Kay, J. E., Chepfer, H., English, J. M., and deBoer G.: Ubiquitous low-level liquid-containing Arctic clouds: New observations and climate model constraints from CALIPSO-GOCCP, Geophys. Res. Lett., 39, L20804, doi:10.1029/2012GL053385, 2012.

Cesana, G., and Chepfer, H.: Evaluation of the cloud water phase in a climatemodel using CALIPSO-GOCCP, J. Geophys. Res. Atmos, 118, 7922–7937, doi:10.1002/jgrd.50376, 2013.

Cesana, G., Waliser, D. E., Jiang, X., and Li, J.-L. F.: Multi-model evaluation of

cloud phase transition using satellite and reanalysis data, J. Geophys. Res. Atmos., 120, 7871–7892, doi:10.1002/2014JD022932, 2015.

Cesana G., Chepfer, H., Winker, D., Cai, X., Getzewich, B., Okamoto, H., Hagihara, Y., Jourdan, O., Mioche, G., Noel, V., and Reverdy, M.: Using in-situ airborne measurements to evaluate three cloud phase products derived from CALIPSO, J. Geophys. Res. Atmos., 121, doi:10.1002/2015JD024334, 2016.

Chepfer, H., Bony, S., Winker, D. M., Chiriaco, M., Dufresne, J.-L., and Seze, G.: Use of CALIPSO lidar observations to evaluate the cloudiness simulated by a climate model, Geophys. Res. Lett., 35, L15704, doi:10.1029/2008GL034207, 2008.

Chepfer, H., Bony, S., Winker, D., Cesana, G., Dufresne, J. L., Minnis, P., Stubenrauch, C. J., and Zeng, S.: The GCM Oriented Calipso Cloud Product (CALIPSO-GOCCP), J. Geophys. Res., 115, D00H16, doi:10.1029/2009JD012251, 2010.

Choi, Y.S., Lindzen, R.S., Ho, C.H., and Kim, J.: Space observations of cold-cloud phase change, Proc. Natl. Acad. Sci. U.S.A., 107, 11, 211–11,216, 2010.

Choi,Y.-S., Ho, C.-H., Park, C.-E., Storelvmo, T., and Tan I.: Influence of cloud phase composition on climate feedbacks, J. Geophys. Res. Atmos., 119, 3687–3700, doi:10.1002/2013JD020582, 2014.

Cziczo, D.J., Froyd, K.D., Hoose, C., Jensen, E.J., Diao, M., Zondlo, M.A., Smith, J.B., Twohy, C.H., and Murphy, D.M.: Clarifying the dominant sources and mechanisms of cirrus cloud formation, Science, 340(6138), 1320–1324, doi:10.1126/science.1234145, 2013.

Dee, D.P., Uppala, S.M., Simmons, A.J., et al.: The ERA‐Interim reanalysis: Configuration and performance of the data assimilation system, Quart. J. Roy. Meteor. Soc., 137(656), 553-597, 2011.

Delanoe, J., and Hogan R. J.: Combined CloudSat–CALIPSO–MODIS retrievals of the properties of ice clouds, Journal of Geophysical Research–Atmospheres, 115, D00H29, doi:10.1029/2009JD012346, 2010.

DeMott, P.J., Prenni, A.J., Liu, X., et al.: Predicting global atmospheric ice nuclei distributions and their impacts on climate, Proc. Natl. Acad. Sci. U. S. A., 107(25), 11217-11222, 2010.

Forbes, R.M., and Ahlgrimn, M.: On the Representation of High-Latitude Boundary Layer Mixed-Phase Cloud in the ECMWF Global Model, Mon. Weather Rev.,142, 3425-3445, DOI: 10.1175/MWR-D-13-00325.1, 2014.

Findeisen, W.: The evaporation of cloud and raindrops, Meteor. Z., 56, 453–460, 1939.

Hogan, R.J., Illingworth, A.J., O'Connor, E.J., and Poiares Baptista, J.P.V.: Characteristics of mixed-phase clouds. II: A climatology from ground-based lidar, Quart. J. Roy. Meteor. Soc., 129, 2117–2134, 2003.

Hu, Y., Vaughan, M., Liu, Z., Lin, B., Yang, P., Flittner, D., Hunt, W., Kuehn, R., Huang, J., Wu, D., Rodier, S., Powell, K., Trepte, C., and Winker, D.: The depolarization-attenuated backscatter relation: CALIPSO lidar measurements vs. theory, Opt. Exp., 15, 5327–5332, 2007.

Hu, Y., Winker, D., Vaughan, M., Lin, B., Omar, A., Trepte, C., Flittner, D., Yang, P., Nasiri, S., Baum, B. A., Sun, W., Liu, Z., Wang, Z., Young, S., Stamnes, K., Huang, J., Kuehn, R., and Holz, R. E.: CALIPSO/ CALIOP cloud phase discrimination algorithm, J. Atmos. Ocean. Technol., 26, 2206–2309. DOI:10.1175/2009JTECHA1280.1, 2009.

Hu, Y., Rodier, S., Xu, K.M., Sun,W., Huang, J., Lin, B., Zhai, P., and Josset, D.: Occurrence, liquid water content, and fraction of supercooled water clouds from combined CALIOP/IIR/MODIS measurements, J. Geophys. Res., 115, D00H34, doi:10.1029/2009JD012384, 2010.

Huang, J. P., Minnis, P., and Lin, B.: Advanced retrievals of multilayered cloud properties using multispectral measurements, J. Geophys. Res., 110, D15S18, doi:10.1029/2004JD005101, 2005.

Huang, J. P., Minnis, P., and Lin, B.: Determination of ice water path in ice-over-water cloud systems using combined MODIS and AMSR-E measurements, Geophys. Res. Lett., 33, L21801, doi:10.1029/ 2006GL027038, 2006a.

Huang, J.P., Lin, B., Minnis, P., Wang, T., Wang, X., Hu, Y., Yi, Y., and Ayers, J.R.: Satellite-based assessment of possible dust aerosols semi-direct effect on cloud water path over East Asia, Geophys. Res. Lett., 33, L19802, doi: 10.1029/2006GL026561, 2006b.

Huang, J.P., Minnis, P., Lin, B., Wang, T., Yi, Y., Hu, Y., Sun-Mack, S., and Ayers, K.: Possible influences of Asian dust aerosols on cloud properties and radiative forcing observed from MODIS and CERES, Geophys. Res. Lett., 33, L06824, doi: 10.1029/2005GL024724, 2006c.

Huang, J.P., Minnis, P., Chen, B., Huang, Z., Liu, Z., Zhao, Q., Yi, Y., and Ayers, J. K.: Long-range transport and vertical structure of Asian dust from CALIPSO and surface measurements during PACDEX, *J. Geophys. Res*., *113*, D23212, doi:10.1029/2008JD010620, 2008.

Huang, J.P., Wang, T., Wang, W., Li, Z., and Yan, H.: Climate effects of dust aerosols over East Asian arid and semiarid regions, J. Geophys. Res., 119, 11398–11416, doi:10.1002/2014JD021796, 2014.

Huang, Z., Huang, J., Bi, J., Wang, G., Wang, W., Fu, Q., Li, Z., Tsay, S.-C., and Shi, J.: Dust aerosol vertical structure measurements using three MPL lidars during 2008 China-U.S. joint dust field experiment, J. Geophys. Res., 115 D00K15, doi:10.1029/2009JD013273, 2010.

Intrieri, J.M., Shupe, M.D., Uttal, T., and McCarty, B.J.: An annual cycle of Arctic cloud characteristics observed by radar and lidar at SHEBA, J. Geophys. Res., 107, 8030, doi:10.1029/2000JC000423, 2002.

Jiang, H., Cotton, W. R., Pinto, J. O., Curry, J. A., and Weiss-bluth, M. J.: Cloud resolving simulations of mixed-phase Arctic stratus observed during BASE: Sensitivity to concentration of ice crystals and large-scale heat and moisture advection, J. Atmos. Sci., 57, 2105–2117, 2000.

Kawamoto, K., Suzuki, K.: Microphysical transition in water clouds Over the Amazon and China derived from space-borne radar and Radiometer data, J. Geophys. Res., 117, D05212. http://dx.doi.org/10.1029/2011JD016412, 2012.

Kawamoto, K., Suzuki, K.: Comparison of water cloud microphysics over

mid-latitude land and ocean using CloudSat and MODIS observations, J. Quant. Spectrosc. Radiat. Transf., 122, 13–24, 2013.

Klein, S. A. and Hartmann, D. L.: The seasonal cycle of low stratiform clouds, J. Clim., 6, 1588–1606, 1993.

Li, J., Yi, Y., Minnis, P., Huang, J., Yan, H., Ma, Y., Wang, W., Ayers, J. K.: Radiative effect differences between multi-layered and single-layer clouds derived from CERES, CALIPSO, and CloudSat data, J. Quant. Spectrosc. Radiat. Transf., 112, doi:10.1016/j.jqsrt.2010.10.006, 2010.

Li, J., Hu, Y., Huang, J., Stamnes, K., Yi, Y., and Stamnes, S.: A new method for retrieval of the extinction coefficient of water clouds by using the tail of the CALIOP signal, Atmos. Chem. Phys., 11, 1-15, 2011.

Li, J., Yi, Y. H., Stamnes, K., Ding, X. D., Wang, T. H., Jin, H. C., and Wang, S. S.: A new approach to retrieve cloud base height of marine boundary layer clouds, Geophys. Res. Lett., 40, 4448–4453, doi:10.1002/grl.50836, 2013.

Li, J., Huang, J., Stamnes, K., Wang, T., Lv, Q., and Jin, H.: A global survey of cloud overlap based on CALIPSO and CloudSat measurements, Atmos. Chem. Phys., 15, 519-536, doi:10.5194/acp-15-519-2015, 2015.

Liu, Y., Huang, J., Shi, G., Takamura, T., Khatri, P., Bi, J., Shi, J.,Wang, T., Wang, X., and Zhang, B.: Aerosol optical properties and radiative effect determined from sky-radiometer over Loess Plateau of Northwest China, Atmos. Chem. Phys., 11, 11455–11463, doi:10.5194/acp-11-11455-2011, 2011.

Liu, Z., Vaughan, M., Winker, D., Kittaka, C., Getzewich, B., Kuehn, R., Omar, A., Powell, K., Trepte, C., and Hostetler, C.:The CALIPSO lidar cloud and aerosol discrimination: Version 2 algorithm and initial assessment of performance, J. Atmos. Oceanic Technol., 26(7), 1198–1213, doi:10.1175/2009JTECHA1229.1, 2009.

Lv, Q., Li, J., Wang, T., and Huang, J.: Cloud radiative forcing induced by layered clouds and associated impact on the atmospheric heating rate, J. Meteor. Res., 29(5), 779-792, doi: 10.1007/s13351-015-5078-7, 2015.

McCoy, D.T., Hartmann, D. L., and Grosvenor, D.P.: Observed Southern Ocean

Cloud Properties and Shortwave Reflection Part 2: Phase changes and low cloud feedback, J. Climate, 27, 8858-8868, doi:10.11175/JCLI-D-14-00288.1, 2014.

McCoy, D.T., Hartmann, D. L., Zelinka, M.D., Ceppi, P., and Grosvenor, D.P.: Mixed-phase cloud physics and Southern Ocean cloud feedback in climate models, J. Geophys. Res. Atmos., doi: 10.1002/2015JD023603, 9539-9554, 2015.

Mielonen, T., Arola, A., Komppula, M., Kukkonen, J., Koskinen, J., Leeuw, G. de., and Lehtinen, K. E. J.: Comparison of CALIOP level 2 aerosol subtypes to aerosol types derived from AERONET inversion data, Geophys. Res. Lett., 36, L18804, doi:10.1029/2009GL039609, 2009.

Moeng, C.-H.: Entrainment rate, cloud fraction, and liquid water path of PBL stratocumulus cloud. J. Atmos. Sci., 57, 3627–3643, doi:10.1175/1520-0469, 2000.

Morrison, A. E, Siems, S.T, and Manton, M. J.: A three-year climatology of cloud-top phase over the Southern Ocean and North Pacific, J. Clim., 24(9), 2405-2418, 2011.

Naud, C.M., Del Genio, A.D., and Bauer, M.: Observational constraints on the cloud thermodynamic phase in midlatitude storms, J. Clim., 19(20), 5273-5288, 2006.

Niedermeier, D., et al.: Experimental study of the role of physicochemical surface processing on the IN ability of mineral dust particles, Atmos. Chem. Phys., 11(21), 11,131–11,144, doi:10.5194/acp-11-11131-2011, 2011.

Noel, V., and Chepfer, H.: A global view of horizontally oriented crystals in ice clouds from Cloud‐Aerosol Lidar and Infrared Pathfinder Satellite Observation (CALIPSO), J. Geophys. Res., 115, D00H23, doi:10.1029/2009JD012365, 2010.

Omar, A. H., et al.: The CALIPSO automated aerosol classification and lidar ratio selection algorithm, J. Atmos. Oceanic Technol., 26(10), 1994–2014, doi:10.1175/2009JTECHA1231.1, 2009.

Pinto, J. O.: Autumnal mixed-phase cloudy boundary layers in the Arctic, J. Atmos. Sci., 55, 2016–2038, 1998.

Pruppacher, H. R., and Klett, J. D.:Microphysics of Clouds and Precipitation, 2nd ed.,

954 pp., Kluwer Acad., Dordrecht, Netherlands, 1997.

Rauber, R. M., and Tokay, A.: An explanation for the existence of supercooled water at the top of cold clouds, J. Atmos. Sci., 48, 1005–1023, 1991.

Richardson, M. S., et al.: Measurements of heterogeneous ice nuclei in the western United States in springtime and their relation to aerosol characteristics, J. Geophys. Res., 112, D02209, doi:10.1029/2006JD007500, 2007.

Sassen, K.: Evidence of liquid phase cirrus cloud formation from volcanic aerosols: Climate implications, Science, 257, 516–519, 1992.

Sassen, K., and Khvorostyanov, V.I.: Microphysical and radiative properties of mixed phase altocumulus: a model evaluation of glaciation effects. Atmos. Res., 84, 390–398, 2007.

Shupe, M.D., Matrosov, S.Y., and Uttal, T.: Arctic mixed-phase cloud properties derived from surface-based sensors at SHEBA, J. Atmos. Sci., 63(2), 697-711, 2006.

Shupe, M. D., Kollias, P., Persson, P. O. G., and McFarquhar, G. M.: Vertical motions in arctic mixed phase stratus, J. Atmos. Sci., 65,1304–1322, 2008.

Stephens, G.L., Vane, D.G., Boain, R.J., Mace, G.G., Sassen, K., Wang, Z., Illingworth, A.J., O'Connor, E.J., Rossow, W.B., Durden, S.L., Miller, S.D., Austin, R.T., Benedetti, A., Mitrescu, C., and CloudSat Science Team.: The CloudSat mission and the A-Train, A new dimension of space-based observations of clouds and precipitation, B. Am. Meteorol. Soc., 83, 1771–1790, 2002.

Su, J., Huang, J., Fu, Q., Minnis, P., Ge, J., and Bi, J.: Estimation of Asian dust aerosol effect on cloud radiation forcing using Fu-Liou radiative model and CERES measurements, Atmos. Chem. Phys., 8, 2763-2771, 2008.

Sun, Z., and Shine, K. P.: Studies of the radiative properties of ice and mixed-phase clouds, Quart. J. Roy. Meteor. Soc.,120, 111–137, 1994.

Tan, I., Storelvmo, T., and Choi, Y.S.: Spaceborne lidar observations of the ice-nucleating potential of dust, polluted dust and smoke aerosols in mixed-phase

clouds, J. Geophys. Res. Atmos., 119, 6653–6665, doi:10.1002/2013JD021333, 2014.

Tremblay, A., Glazer, A., Yu, W., and Benoit, R.: A mixed-phase cloud scheme based on a single prognostic equation, Tellus, 48A, 483–500, 1996.

Tsushima, Y., Emori, S., Ogura, T., Kimoto, M., Webb, M. J., Williams, K. D., Ringer, M. A., Soden, B. J., Li, B., and Andronova, N.: Importance of the mixed phase cloud distribution in the control climate for assessing the response of clouds to carbon dioxide increase: a multi‐model study, Clim. Dyn., 27, 113–126, 2006.

Wang, W., Huang, J., Minnis, P., Hu, Y., Li, J., Huang, Z., Ayers,J. K., and Wang, T.: Dusty cloud properties and radiative forcing over dust source and downwind regions derived from A-Train data during the Pacific Dust Experiment, J. Geophys. Res., 115, D00H35, doi:10.1029/2010JD014109, 2010.

Wang, W., Sheng, L., Jin, H., and Han. Y.: Dust Aerosol Effects on Cirrus and Altocumulus Clouds in Northwest China, J. Meteor. Res., 29 (5): 793-805, 2015.

Wang, W., Sheng, L., Dong, X., Qu, W., Sun, J., Jin, H., and Logan, T.: Dust aerosol impact on the retrieval of cloud top height from satellite observations of CALIPSO, CloudSat and MODIS, J. Quant. Spectrosc. Radiat. Transf., doi:10.1016/j.jqsrt.2016.03.034, 2016.

Wegener, A.: Thermodynamik der Atmosphäre. JA Barth, 331 pp, 1911.

West, R. E. L., Stier, P., Jones, A., Johnson, C. E., Mann, G. W., Bellouin, N., Partridge, D. G., and Kipling Z.: The importance of vertical velocity variability for estimates of the indirect aerosol effects, Atmos. Chem. Phys., 14, 6369–6393, doi:10.5194/acp-14-6369-2014, 2014.

Westbrook, C. D., Illingworth, A. J., O'Connor, E. J., and Hogan R. J.: Doppler lidar measurements of oriented planar ice crystals falling from supercooled and glaciated layer clouds, Q. J. R. Meteorol. Soc.,136, 260–276, 2010.

Winker D. M., Hunt, W. H., and Mcgill, M. J.: Initial performance assessment of

CALIOP, Geophys. Res. Lett., 34, L19803, doi:10.1029/ 2007GL030135, 2007.

Wood, R.: Stratocumulus clouds, *Mon. Wea. Rev.*, 140, 2373-2423, 2012.

Yuan, T. and Oreopoulos, L.: On the global character of overlap between low and high clouds, Geophys. Res. Lett., 40, 5320–5326, doi:10.1002/grl.50871, 2013.

Zhang, D., Wang, Z., and Liu D.: A global view of midlevel liquid-layer topped stratiform cloud distribution and phase partition from CALIPSO and CloudSat measurements, J. Geophys. Res., 115, D00H13, doi: 10.1029/2009JD012143, 2010.

Zhang, D., Liu, D., Luo, T., Wang, Z., and Yin, Y.: Aerosol impacts on cloud thermodynamic phase change over East Asia observed with CALIPSO and CloudSat measurements, J. Geophys. Res. Atmos., 120, 1490–1501, doi:10.1002/2014JD022630, 2015.

Table1. The summary of spatial correlation coefficients between SCFs and meteorological parameters at three isotherms under different aerosol loading conditions. Only regions with temporal correlations between SCFs and meteorological parameters at the 90% confidence level are used to calculate the spatial correlations between SCFs and meteorological parameters.

Isotherm(℃)		**-10**			**-20**			**-30**	
	HAL[a]	**MAL[a]**	**LAL[a]**	**HAL**	**MAL**	**LAL**	**HAL**	**MAL**	**LAL**
Velocity (tropics)	0.97	0.97	0.99	0.98	0.99	0.97	0.98	0.24	0.6
								P=0.66[b]	**P=0.23**
RH (tropics)	0.99	0.99	0.97	0.95	0.96	0.97	0.47	0.43	0.36
							P=0.23	**P=0.47**	**P=0.4**
ST (tropics)	0.21	0.38	-0.44	-0.08	-0.2	-0.58	NaN	-0.55	-0.94
	P=0.7	**P=0.2**	**P=0.35**	**P=0.67**	**P=0.15**	**P=0.16**		**P=0.15**	
U wind-SH	0.92	0.96	-0.85	0.92	0.87	0.89	NaN	-0.34	-0.87
								P=0.35	
U wind-NH	-0.8	0.92	0.95	0.85	0.93	0.9	0.91	0.94	0.93
LTSS-SH	-0.95	-0.92	-0.99	-0.94	-0.99	-0.36	NaN	-0.92	-0.91
						P=0.85			
LTSS-NH	-0.94	-0.92	-0.91	0.51	0.51	0.87	0.61	0.58	0.82
				P=0.29	**P=0.26**		**P=0.54**	**P=0.4**	
ST-SH	-0.8	-0.7	0.51	-0.97	-0.97	-0.91	NaN	-0.03	0.98
		P=0.13	**P=0.12**					**P=0.89**	
ST-NH	0.7	**-0.7**	**0.47**	-0.95	-0.95	-0.93	-0.99	-0.92	-0.98
	P=0.13	**P=0.2**	**P=0.34**						

[a] HAL, MAL and LAL are represent the high, middle and low aerosol loading level; [b] We also provide the confidence value (i.e., p value) when the confidence level of the spatial correlation between variables is less than 90%.

Figure Captions

Fig.1. The global and seasonal variations of supercooled water cloud fractions (SCFs) and relative aerosol frequencies (RAFs) at -10 ℃ isotherm over 2 °×2 °grid boxes.

Fig.2. The global and seasonal variations of supercooled water cloud fractions (SCFs) and relative aerosol frequencies (RAFs) at -20 ℃ isotherm over 2 °×2 °grid boxes.

Fig.3. The global and seasonal variations of supercooled water cloud fractions (SCFs) and relative aerosol frequencies (RAFs) at -30 ℃ isotherm over 2 °×2 °grid boxes.

Fig.4. The zonal and seasonal variations of SCFs and RAFs at -20 ℃ isotherm.

Fig.5. Temporal correlations (at the 90% confidence level) between SCFs at three isotherms and skin temperature (left panel) and vertical velocity at 500 hPa (right panel). The correlations are based on 96 months' monthly SCF and meteorological parameters. Grid size is: 6 °latitude by 6 °longitude.

Fig.6. Similar with Fig.5, but is for relative humidity (left panel) and LTSS (right panel).

Fig.7. Similar with Fig.5, but is for u wind at 100 hPa.

Fig.8. Time series plots of SCFs, meteorological parameters and RAFs of IN aerosol at -30 ℃ isotherm over the central China (102 °E-108 °E, 30 °N-36 °N). Each line in every subplot corresponds to a time series of different variables after 5 months of smoothing. The coefficients (at the 90% confidence level) in subplots represent the temporal correlation between the original SCFs series and meteorological parameters (or RAFs). The confidence values (i.e., p value) are provided only when the confidence level of the temporal correlation between variables is less than 90%.

Fig.9. Similar with Fig.8, but is for -10 ℃ isotherm over a region near the Bahamas (66 ℃W-60 ℃W, 18 ℃N-12 ℃N).

Fig.10. Similar with Fig.8, but is for -20 ℃ isotherm over the southern ocean (84 ° E-90 ℃E, 54 ℃S-60 ℃S).

Fig.11. Spatial correlations between SCFs at -20 ℃ isotherm and meteorological parameters under different aerosol loading conditions. Left panel represents tropics, whereas middle and right panels correspond to the correlations in middle and high latitudes of northern and southern hemispheres, respectively. Only those regions with temporal correlations between SCFs and meteorological parameters at the 90% confidence level are used to calculate the spatial correlations between SCFs and meteorological parameters. The correlation coefficients are provided in Table 1.

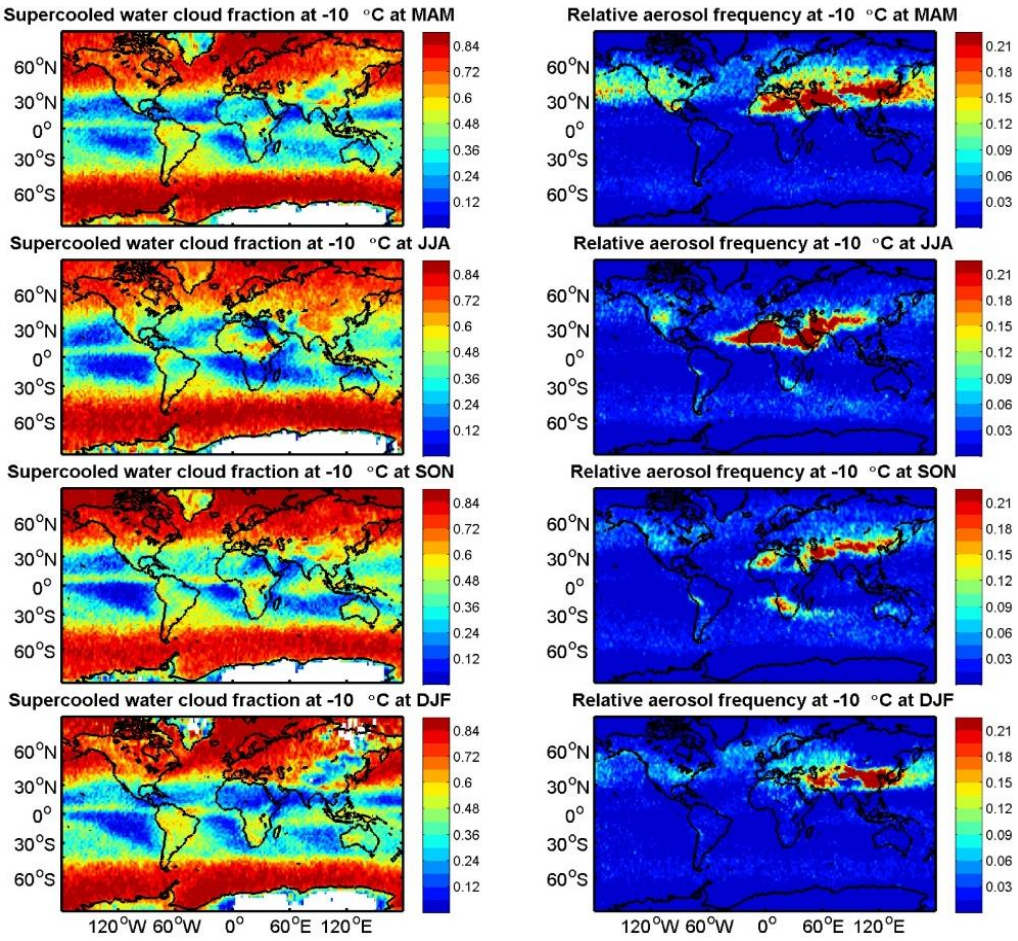

995 **Fig.1.** The global and seasonal variations of supercooled water cloud fractions (SCFs) and relative aerosol frequencies (RAFs) at -10 ℃ isotherm over 2 °×2 °grid boxes.

1000

1005

1010

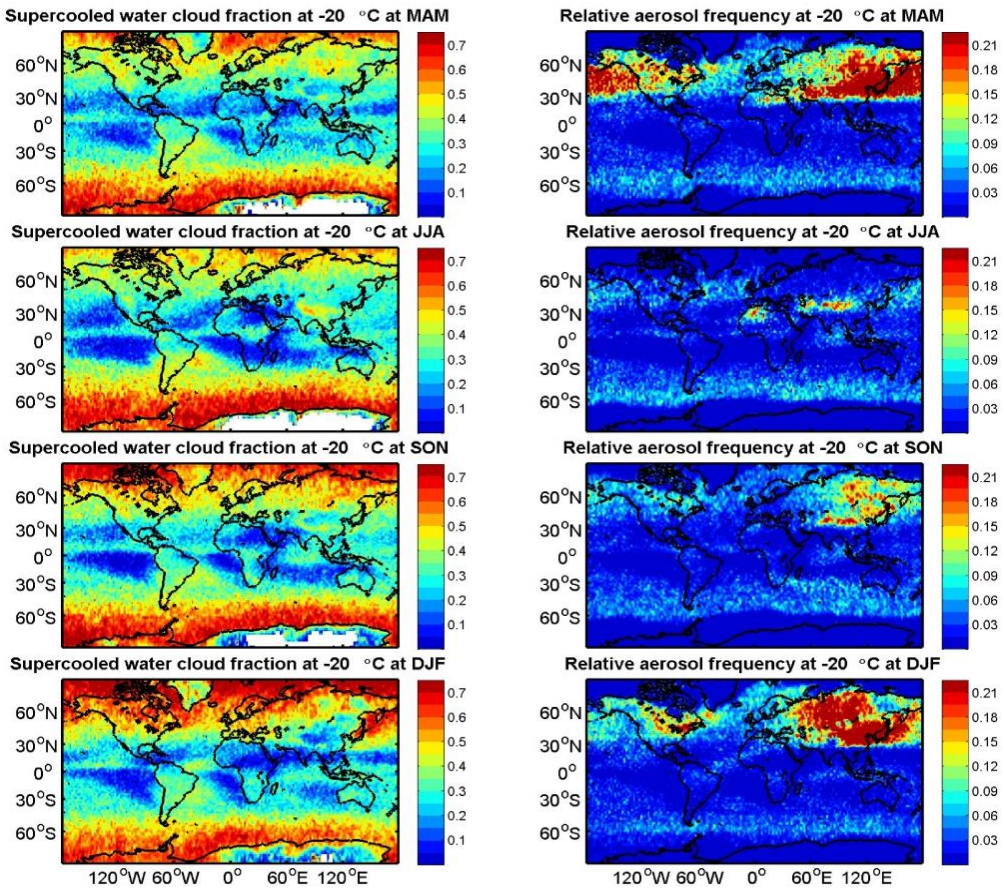

Fig.2. The global and seasonal variations of supercooled water cloud fractions (SCFs) and relative aerosol frequencies (RAFs) at -20 ℃ isotherm over 2 °×2 °grid boxes.

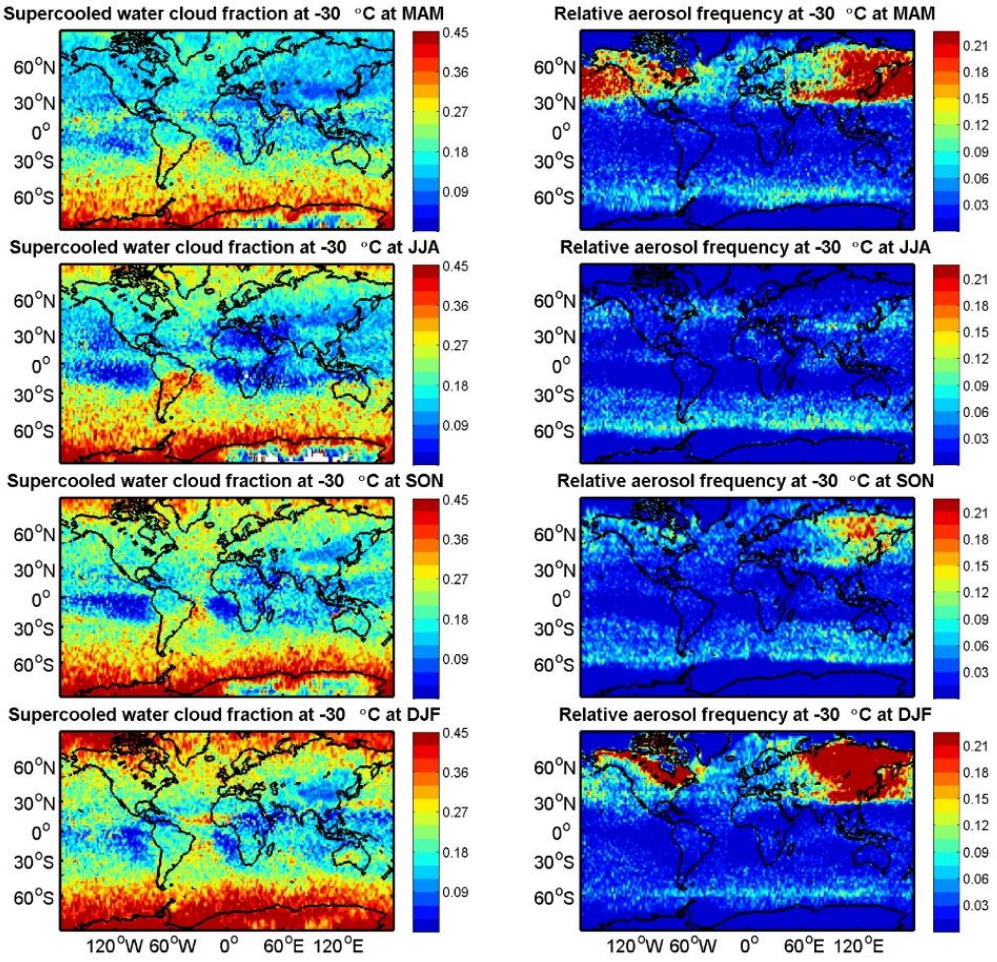

1035

Fig.3. The global and seasonal variations of supercooled water cloud fractions (SCFs) and relative aerosol frequencies (RAFs) at -30 ℃ isotherm over 2 °×2 °grid boxes.

1040

1045

1050

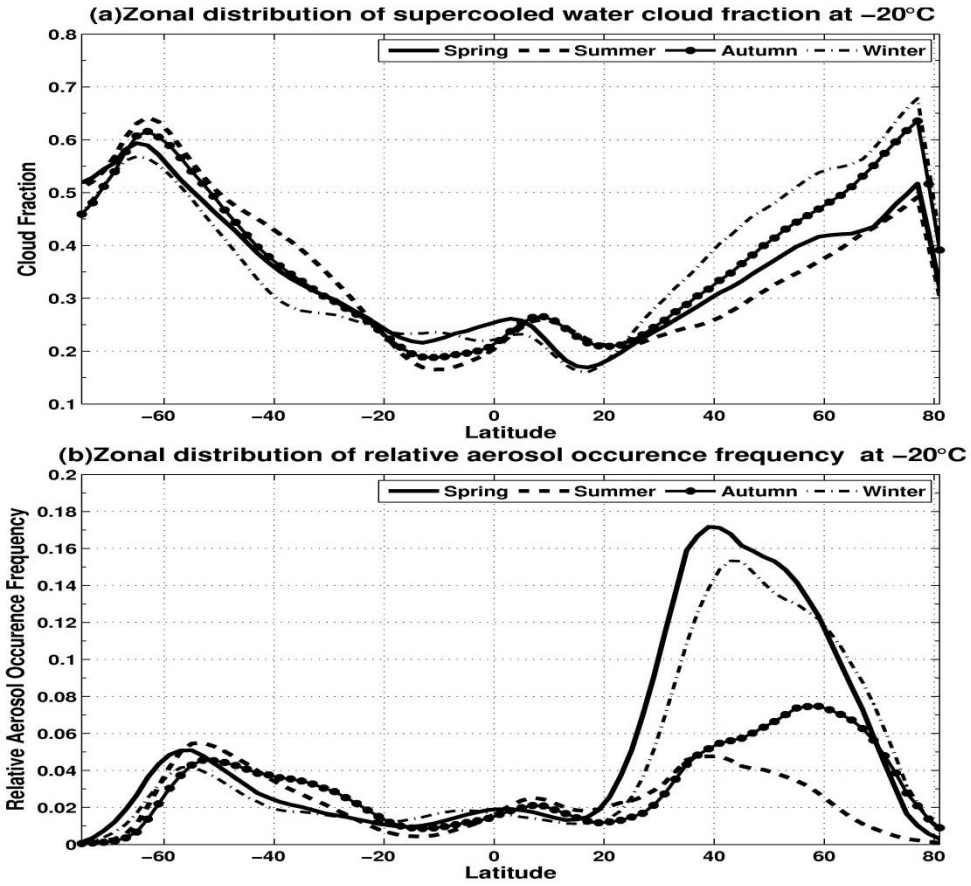

Fig.4. The zonal and seasonal variations of SCFs and RAFs at -20 ℃ isotherm.

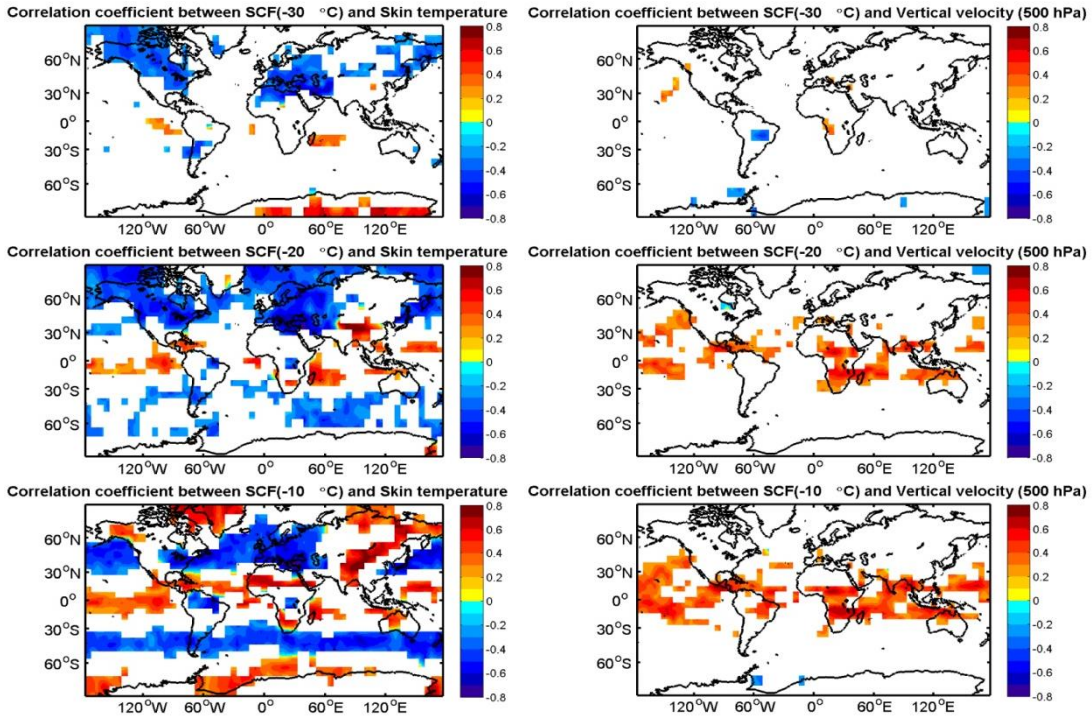

Fig.5. Temporal correlations (at the 90% confidence level) between SCFs at three isotherms and skin temperature (left panel) and vertical velocity at 500 hPa (right panel). The correlations are based on 96 months' monthly SCF and meteorological parameters. Grid size is: 6 ºlatitude by 6 ºlongitude.

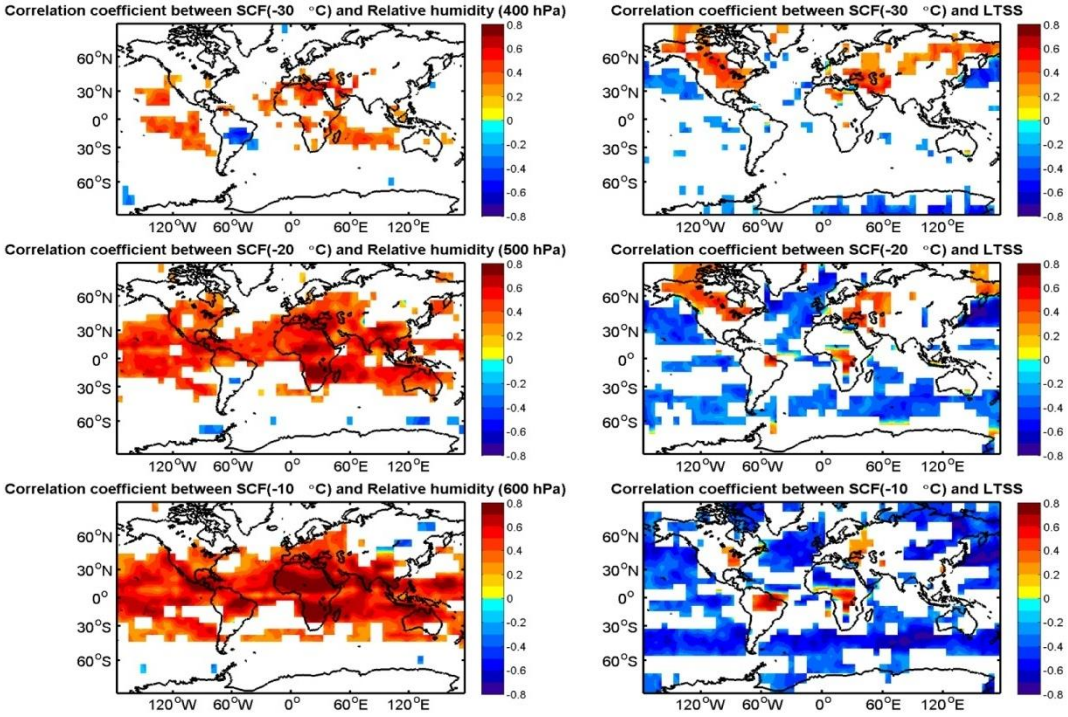

Fig.6. Similar with Fig.5, but is for relative humidity (left panel) and LTSS (right panel).

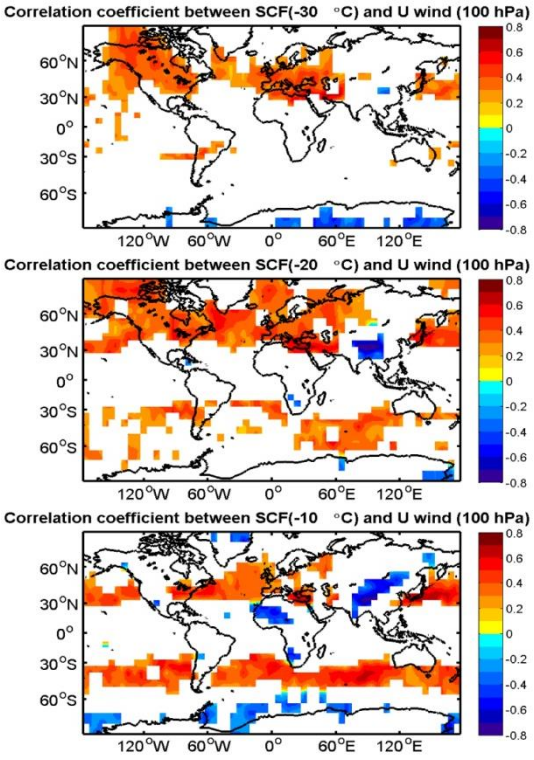

Fig.7. Similar with Fig.5, but is for u wind at 100 hPa.

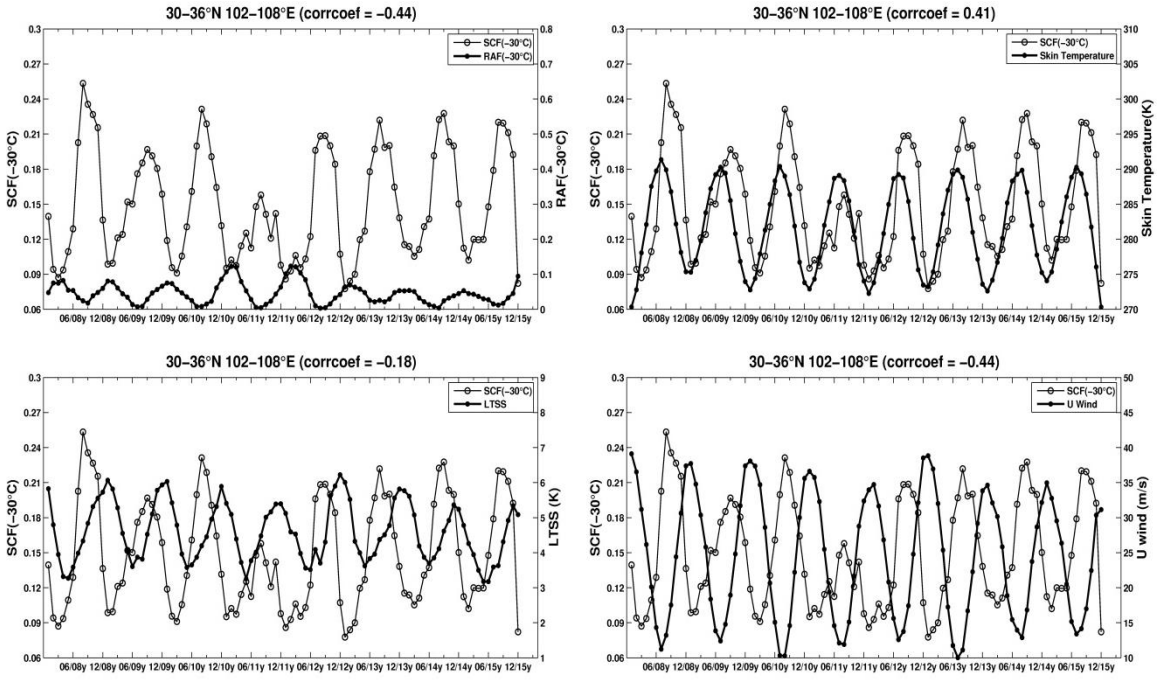

Fig.8. Time series plots of SCFs, meteorological parameters and RAFs of IN aerosol at -30 ℃ isotherm over the central China (102 ℃E-108 ℃E, 30 ℃N-36 ℃N). Each line in every subplot corresponds to a time series of different variables after 5 months of smoothing. The coefficients (at the 90% confidence level) in subplots represent the temporal correlation between the original SCFs series and meteorological parameters (or RAFs). The confidence values (i.e., *p* value) are provided only when the confidence level of the temporal correlation between variables is less than 90%.

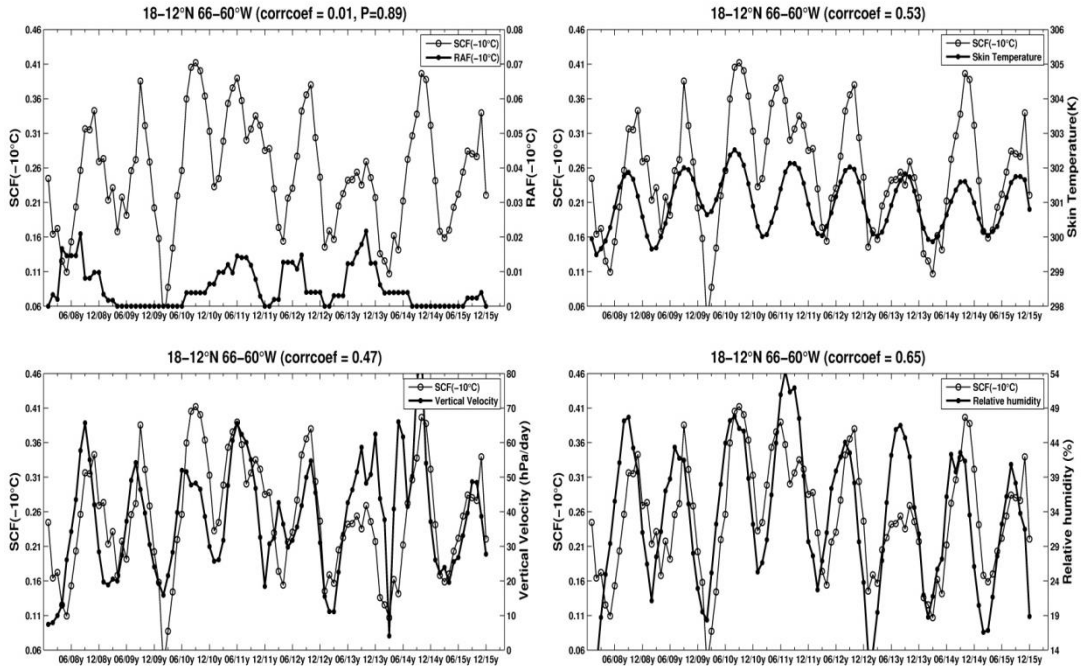

Fig.9. Similar with Fig.8, but is for -10 ℃ isotherm over a region near the Bahamas (66 ℃W-60 ℃W, 18 ℃N-12 ℃N).

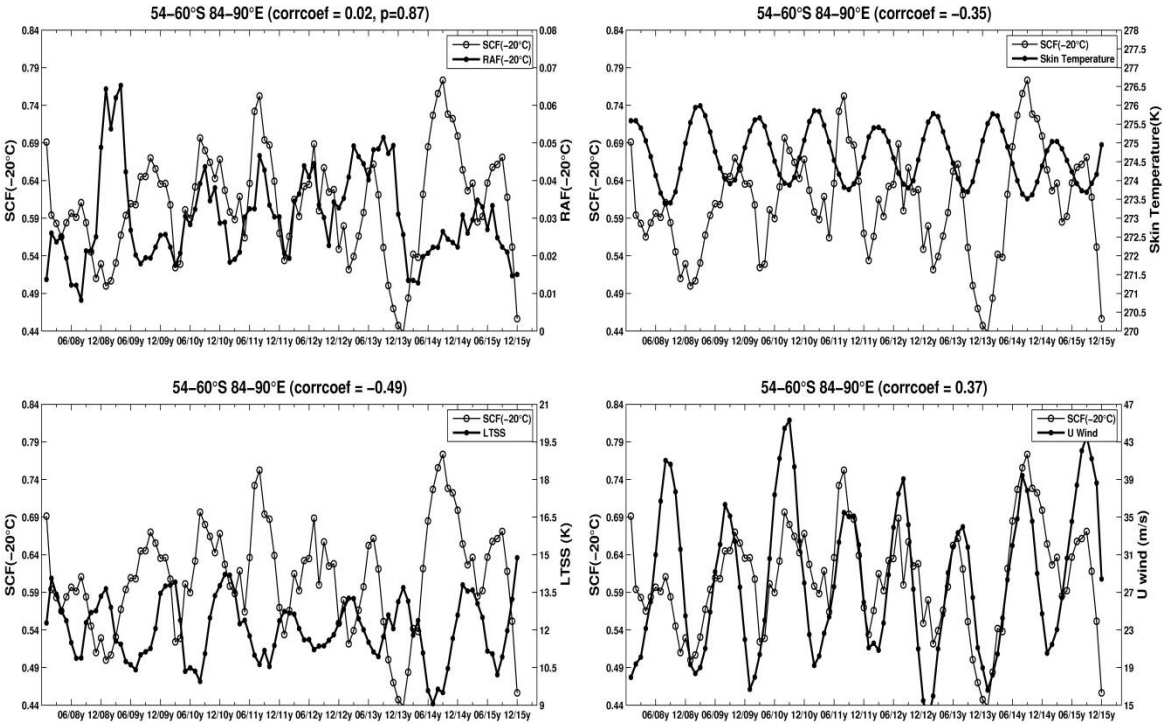

Fig.10. Similar with Fig.8, but is for -20 ℃ isotherm over the southern ocean (84 ° E-90 ℃E, 54 ℃S-60 ℃S).

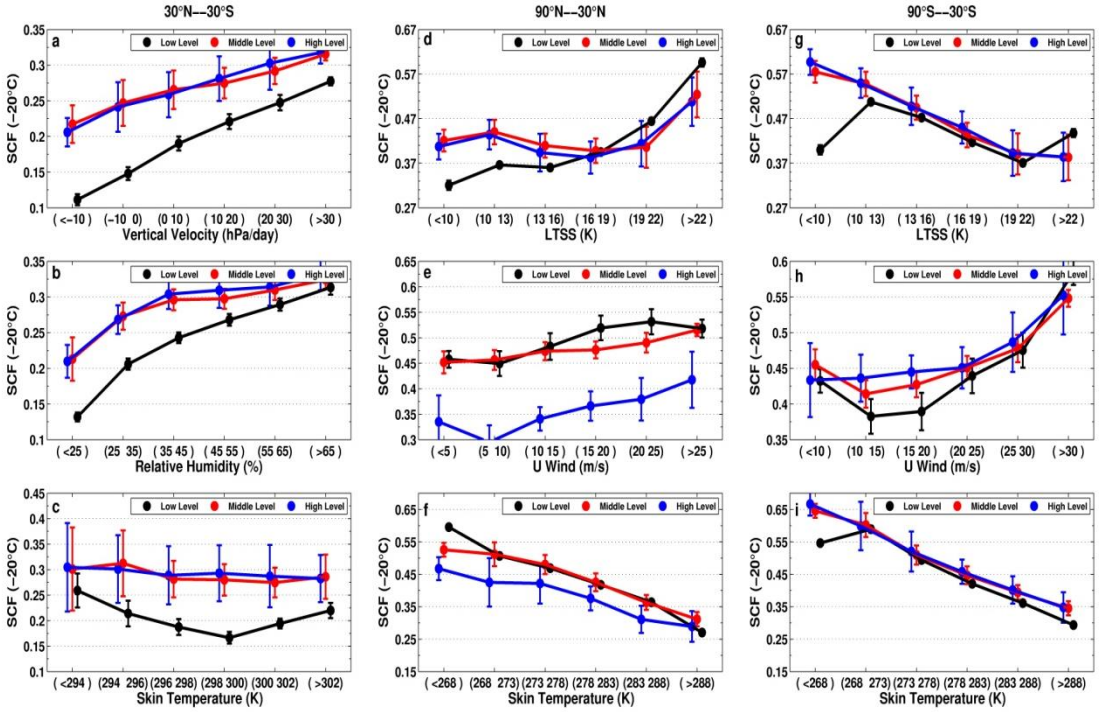

Fig.11. Spatial correlations between SCFs at -20 ℃ isotherm and meteorological parameters under different aerosol loading conditions. Left panel represents tropics, whereas middle and right panels correspond to the correlations in middle and high latitudes of northern and southern hemispheres, respectively. Only those regions with temporal correlations between SCFs and meteorological parameters at the 90% confidence level are used to calculate the spatial correlations between SCFs and meteorological parameters. The correlation coefficients are provided in Table 1.